Magn Reson Med Sci 2017; 16; 253–258
doi:10.2463/mrms.tn.2016-0149
Published Online: September 30, 2016

TECHNICAL NOTE

An Asymmetric Birdcage Coil for Small-animal MR Imaging at 7T

Kyoung-Nam Kim[1], Sang-Doc Han[1], Jeung-Hoon Seo[1], Phil Heo[2], Dongkyeom Yoo[1], Geun Ho Im[1], and Jung Hee Lee[2,3*]

The birdcage (BC) coil is currently being utilized for uniform radiofrequency (RF) transmit/receive (Tx/Rx) or Tx-only configuration in many magnetic resonance (MR) imaging applications, but insufficient magnetic flux ($|B_1|$) density and their non-uniform distribution still exists in high-field (HF) environments. We demonstrate that the asymmetric birdcage (ABC) transmit/receive (Tx/Rx) volume coil, which is a modified standard birdcage (SBC) coil with the end ring split into two halves, is suitable for improving the $|B_1|$ sensitivity in 7T small-animal MR imaging. Cylindrical SBC and ABC coils with 35 mm diameter were constructed and bench tested for mouse body MR imaging at 300 MHz using a 7T scanner. To assess the ABC coil performance, computational electromagnetic (EM) simulation and 7T MR experiment were performed by using a cylindrical phantom and *in vivo* mouse body and quantitatively compared with the SBC coil in terms of $|B_1|$ distribution, RF transmit ($|B_1^+|$) field, and signal-to-noise ratio (SNR). The bench measurements of the two BC coils are similar, yielding a quality value (Q-value) of 74.42 for the SBC coil and 77.06 for the ABC coil. The computational calculation results clearly show that the proposed ABC coil offers superior $|B_1|$ field and $|B_1^+|$ field sensitivity in the central axial slice compared with the SBC coil. There was also high SNR and uniformly distributed flip angle (FA) under the loaded condition of mouse body in the 7T experiment. Although ABC geometry allows a further increase in the $|B_1|$ field and $|B_1^+|$ field sensitivity in only the central axial slice, the geometrical modification of the SBC coil can make a high performance RF coil feasible in the central axial slice and also make target imaging possible in the diagonal direction.

Keywords: *magnetic resonance imaging, radiofrequency coil, signal-to-noise ratio, Asymmetric birdcage coil, 7T, $|B_1|$ field*

Introduction

In small-animal magnetic resonance (MR) imaging, high static magnetic field strength ($B_0 \geq 7T$) is suggested because of its inherently derived high signal-to-noise ratio (SNR).[1,2] This is a decisive factor in the ongoing research, but volume radiofrequency (RF) coil for frequency above 300 MHz has specific limitations such as the restriction of tuning frequency given by high inductance value in the RF coil and confined mode spacing between desired mode and undesired mode the gradient mode. The heterogeneous RF field ($|B_1|$) distribution in the imaging region is directly driven by this result.[3,4] In general, the $|B_1|$ field distribution of a volume RF coil is strongly related to the interaction between the RF coil and the subject, which has biological properties such as relative permittivity (ε_r) and conductivity (σ).[5–7] Although unexpected $|B_1|$ field distribution occurs in the high-field (HF) environment, various shapes of volume RF coil, such as end-cap birdcage (BC), helmet shape for closely fitting to the subject, and crown shape designed by curved conducting leg along the B_0-direction, were developed to acquire high resolution MR imaging.[8,9] The BC coil is a popular coil geometry and is currently being utilized in many MR imaging applications by localizing the RF transmit/receive (Tx/Rx) or sizable RF Tx-only configuration.[10,11] However, previous small-animal MR studies using BC coils have been conducted with insufficient $|B_1|$ field sensitivity as well as poor homogeneity. This problem is a major challenging work in the imaging of small sized subjects.[12,13]

[1]Center for Molecular and Cellular Imaging, Samsung Biomedical Research Institute, Seoul, Korea
[2]Department of Health Sciences and Technology, Samsung Advanced Institute for Health Science and Technology, Sungkyunkwan University, 81 Irwon-ro, Gangnam-gu, Seoul, Korea
[3]Department of Radiology, Samsung Medical Center, Sungkyunkwan University School of Medicine, Seoul, Korea

*Corresponding author, Phone: +82-2-3410-6459, Fax: +82-2-3410-0084, E-mail: hijunghee@skku.edu

Received: November 22, 2015 | Accepted: July 13, 2016

The purpose of our study is to improve the $|B_1|$ field sensitivity in the central axial slice that involves modification of the coil geometry of the SBC coil, resulting in an asymmetric BC (ABC) coil configuration. The ABC coil configuration by using specific 25 mm offsetting one half of the SBC coil was shape-selectively designed with proportional correlation between coil dimension and $|B_1|$ field sensitivity in that certain imaging region. The modified coil geometry of the ABC coil is equivalent to the standard BC (SBC) coil except for the end ring (ER) of the SBC coil split into two halves. To evaluate of the performance of the ABC coil, a computational calculation using the finite different time domain (FDTD) and a 7T *in vivo* mouse body MR imaging were performed and compared with the SBC coil in terms of the $|B_1|$ field and RF transmit ($|B_1^+|$) field and the SNR.

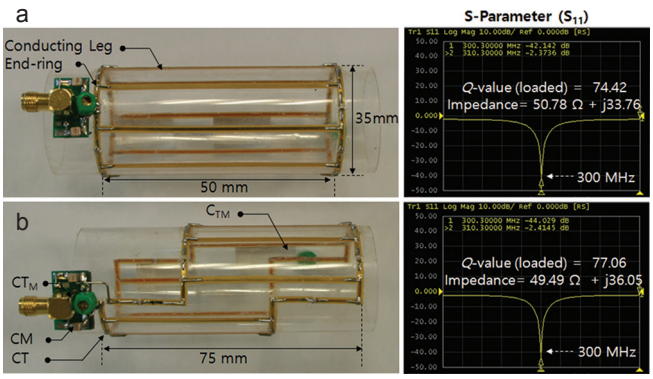

Fig 2. High-pass filter (HPF) version of (**a**) SBC and (**b**) ABC coils, home-built and resonated at 300 MHz, which corresponds to 7T. Electrical performance (right) was determined by measuring the reflection coefficient (S_{11}) in the single port of each BC coil.

Materials and Methods

AutoCAD design of SBC and ABC coils

Figure 1 shows a schematic representation of the SBC (Fig. 1a) and ABC (Fig. 1b) coils designed using the AutoCAD software (Version 2013, Autodesk Inc., San Rafael, California, USA). The dimensions of the eight legs of the SBC coil were a diameter of 35 mm and a length of 50 mm (Fig. 1a). The ABC coil was constructed by offsetting one half of the SBC coil by 25 mm, thus resulting in three sections of equal length across the two halves (Fig. 1b). The two BC coils were wrapped on a cylindrical acrylic former. The ER of each BC coil was interconnected by an electrical capacitor for precise frequency tuning at 300 MHz.

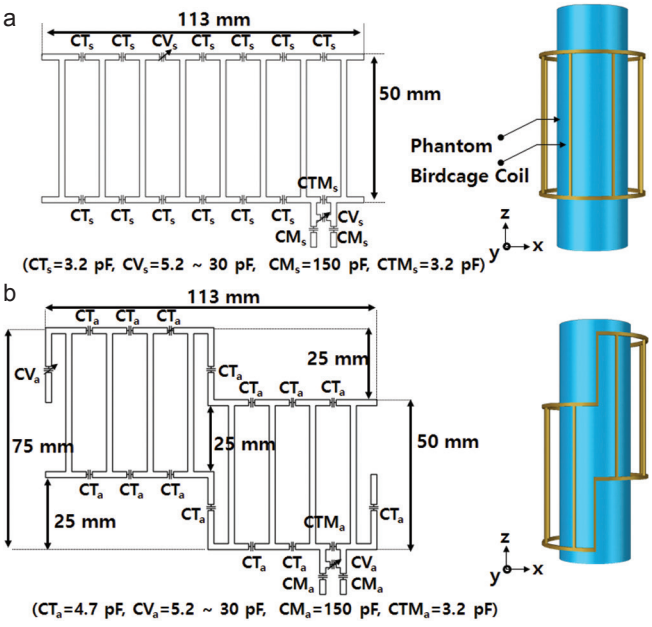

Fig 1. A schematic representation of the (**a**) SBC and (**b**) ABC coils designed using AutoCAD software. The 8-leg high-pass filter (HPF) BC coil was formed using eight copper wires wrapped on a cylindrical former. The ABC coil geometry was constructed by offsetting one half of the SBC coil structure by 25 mm, resulting in three sections of equal length across the two halves.

Figure 2 shows the two constructed BC coils (SBC coil in Fig. 2a and ABC coil in Fig. 2b) with the same high-pass filter (HPF), resonating at 300 MHz, which corresponds to a 7T static magnetic field for proton MR imaging. For conducting magnetic field, the SBC and ABC coils were equipped with a flexible printed circuit board using copper tape (3M Inc., USA), ceramic non-magnetic capacitor (Dalian Dalicap Co., Ltd., China), and double-shielded RG 316 coaxial cable (Belden Inc., USA) on the acrylic former. In addition, to operate in the linear polarization (LP) mode, RG 316 feedlines of 100 mm length were attached to the single port. The copper strip used for the conducting leg and the ER was 1 mm wide and 35 μm thick. For workbench testing, fine tuning of the resonant mode for the two BC coils was accomplished by a tuning capacitor (CTs: 3.2 pF and CTa: 4.7 pF), matching capacitor (CMs and CMa: 150 pF), tuning-matching capacitor (CTMs and CTMa: 3.2 pF), and variable capacitor (CVs and CVa: 5.2 ~ 30 pF) (Fig. 1). The frequency tuning of 300 MHz and 50 Ω matching was adjusted using a network analyzer (Model E5061, Agilent Inc., USA). Electrical performance was determined from the measurement of the reflection coefficient (ρ) in the single port of each BC coil.

Electromagnetic simulation

The eight legs SBC and ABC coils were modeled using a commercial FDTD program (XFdtd, Remcom, Inc., State College, PA, USA). In the geometrical modeling, the SBC and ABC coils were electromagnetically simulated for the same number of capacitors and equal coil diameter (35 mm). A homogeneous cylindrical phantom was modeled with dielectric properties of specific permittivity (ε_r) of 51.95 and conductivity (σ) of 0.55 $S \cdot m^{-1}$. The dimensions of the phantom were a 30 mm diameter and 100 mm length. The entire calculation region was a mesh of 740 mm × 740 mm × 130 mm with a resolution of 1 mm × 1 mm × 1 mm along the x-, y-, and z-directions. During the generation of $|B_1^+|$

field distribution in the simulation, the $|B_1^+|$ field was re-scaled using a specific value of 2 μT in the iso-center of the central axial slice. This value is identical to the 90° RF excitation in the MR experiment. The normalized $|B_1^+|$ field distribution of the SBC and ABC coils was then compared.

Experiments with MRI scanner

All MR imaging experiments were performed on the cylindrical phantom and an *in vivo* mouse body using a 7T Biospec MR scanner (Bruker, Ettlingen, Germany) is equipped with a 200 mm diameter size of magnet bore, a 400 mT/m gradient amplitude and single-channel RF transmit/receive coil configuration. The MR system is connected to the AVIII console running ParaVision 5.1. In the *in vivo* mouse body experiment, cardiac gating was used to eliminate motion artifacts produced by cardiac movement. The MR acquisition parameters were set as follows: three-dimensional (3D) fast low angle shot (FLASH) protocol with a repetition time (TR) of 113.5 ms, echo time (TE) of 3.7 ms, and flip angle (α; FA) of 30°. The field of view (FOV) for obtaining the MR image was chosen as 40 mm × 40 mm for the axial (xy) slice and 80 mm × 40 mm for the sagittal (yz) slice. The FA map and SNR of the SBC and ABC coils were quantitatively compared. In the construction of FA maps, the double angle method (DAM) was used with two different FAs: 30° (α) and 60° (2α). Additionally, the SNR measurement by using the national electrical manufacturers association (NEMA) 4 was performed in the phantom and *in vivo* mouse body axial image.

Results

Workbench test

For the SBC coil, the coil performance characteristics yielded unloaded and loaded gains of −40 dB and −42 dB, respectively, and an impedance of 50.78 Ω in the loaded condition (right picture in Fig. 2a). The corresponding coil performance characteristics of the ABC coil were −41 dB, −44 dB, and 49.49 Ω (right picture in Fig. 2b). The performance of the loaded quality value (Q-value) of the SBC and ABC coils was measured to be 74.42 and 77.06, respectively. The differentiation of the reflection coefficient was ±5% for each coil.

$|B_1^+|$ and $|B_1|$ Field distribution of cylindrical phantom

Figure 3 shows the normalized $|B_1^+|$ and $|B_1|$ field maps of the cylindrical phantom for SBC (Fig. 3a) and ABC (Fig. 3b) coils at 300 MHz. The figure shows field maps for the sagittal (yz) slice in the bilateral direction and for the axial (xy) slice in the central region, for each BC coil. The $|B_1^+|$ and $|B_1|$ fields in the SBC coil (Fig. 3a) show visibly homogeneous distribution in all regions of interest (ROI-1 to ROI-5). On the contrary, the signal intensity (SI) between the center and edge regions in the empty space of the ABC coil loaded with the phantom is low compared with the SBC coil.

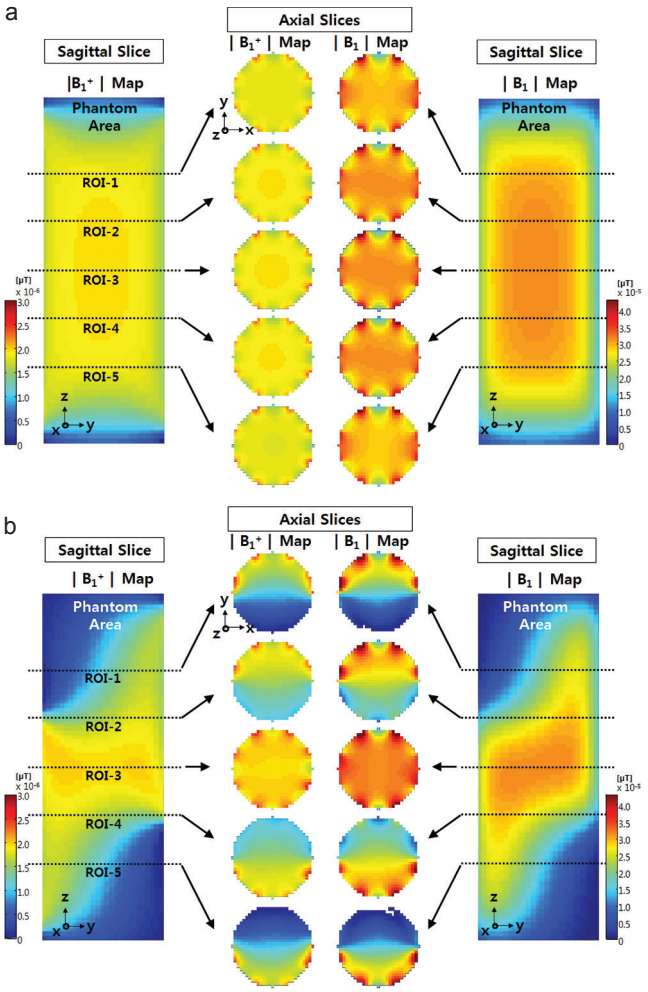

Fig 3. The normalized $|B_1^+|$ and $|B_1|$ fields of a cylindrical phantom for (**a**) SBC and (**b**) ABC coils at 300 MHz, as obtained from the FDTD computational calculation. Each $|B_1^+|$ and $|B_1|$ field map presents five regions of interest (ROIs), in the bilateral direction for the sagittal (yz) slice and in the central region for the axial slice.

Table 1 lists the mean values of the $|B_1^+|$ and $|B_1|$ sensitivities of the two BC coils. In ROI-1 and ROI-5, the ABC coil's $|B_1|$ field sensitivity is lower than that of the SBC coil by ~73% and 88%, respectively. Moreover, in the all ROIs, the ABC coil shows inhomogeneous $|B_1|$ and $|B_1^+|$ sensitivities. However, the mean $|B_1^+|$ and $|B_1|$ signal values of the ABC coil are higher, by 6% each, in the central axial slice of ROI-3 compared with the SBC coil.

Experiments in the 7T MR scanner

Figure 4 shows the FA and SNR maps for the phantom for the SBC and ABC coils at 300 MHz obtained at 7T. The five ROIs in the FA and SNR maps are located in intervals of 12 mm. The FA and SBR maps of the SBC coil are uniformly distributed in all ROIs for the loaded condition of cylindrical phantom. Moreover, these distributions of the SBC and ABC coil (Fig. 4) shows similar to computational calculation results (Fig. 3). Overall, field distribution shows

Table 1. Mean values of the $|B_1|$ and $|B_1^+|$ sensitivities and their homogeneity for SBC and ABC coils, measured and compared with the computational calculation

[Unit: μT]

Computational calculation		ROI_1	ROI_2	ROI_3	ROI_4	ROI_5
$\|B_1\|$ Field (Mean)	SBC	2.93e–05	3.01e–05	3.02e–05	3.01e–05	2.92e–05
	ABC	1.69e–05	2.43e–05	3.21e–05	2.35e–05	1.55e–05
$\|B_1^+\|$ Field (Mean)	SBC	1.81e–06	1.86e–06	1.87e–06	1.86e–06	1.80e–06
	ABC	1.07e–06	1.51e–06	1.99e–06	1.49e–06	1.03e–06

upper raw mean values of magnetic flux density ($|B_1|$), lower raw mean values of RF transmit field ($|B_1^+|$)

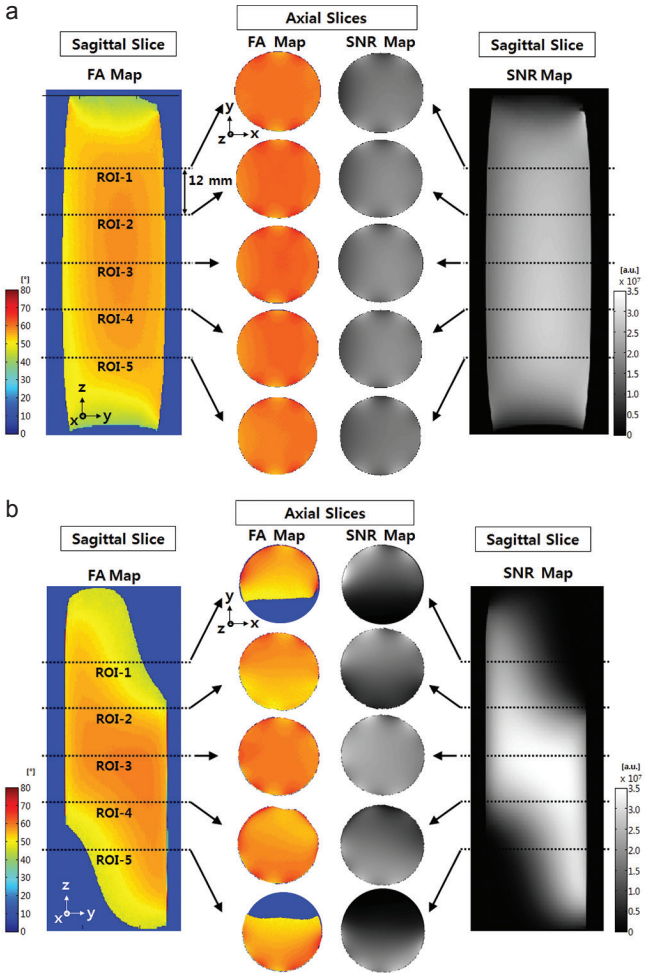

Fig 4. FA and SNR maps for the cylindrical phantom for (**a**) SBC and (**b**) ABC coils at 300 MHz obtained from the 7T MR experiment (left: FA map in sagittal slices, right: SNR map in sagittal slices, Center: Five axial slices of FA and SNR maps (from ROI-1 to ROI-5) located from center to peripheral region per 12 mm distance along the z-direction).

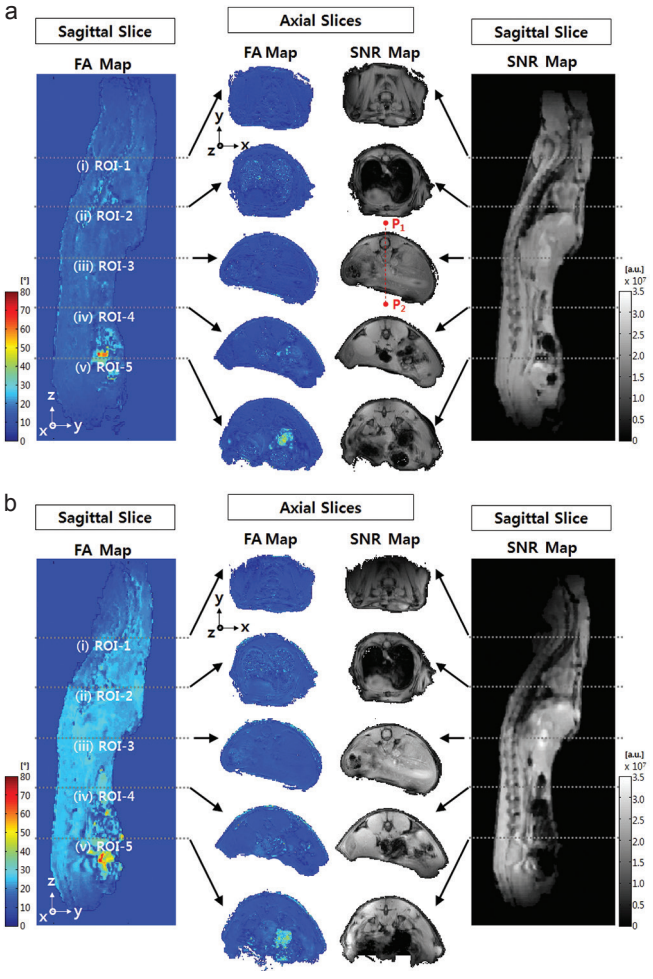

Fig 5. FA and SNR maps for the *in vivo* mouse body for (**a**) SBC and (**b**) ABC coils at 300 MHz obtained from the 7T MR experiment (left : FA map in sagittal slices, right: SNR map in sagittal slices, center: Five axial slices of FA and SNR maps (from ROI-1 to ROI-5) located from center to peripheral region per 12 mm distance along the z-direction).

a rapid decrease in the relative SI in the central axial slice, from ROI-3 to the peripheral ROIs of ROI-1 and ROI-5. However, the FA and SNR maps of ABC coil in ROI-3 show superior performance compared with the SBC coil.

Figure 5 shows the FA and SNR maps of the *in vivo* mouse body for the SBC and ABC coils at 7T. The ABC coil exhibits higher FAs and SNR distribution in the central axial slice of ROI-3 compared with the SBC coil. Although the SI distribution in the central axial slice of the ABC coil is inhomogeneous in ROI-1, ROI-2, ROI-4, and ROI-5, the SI of the SBC coil was measured with a higher SNR signal.

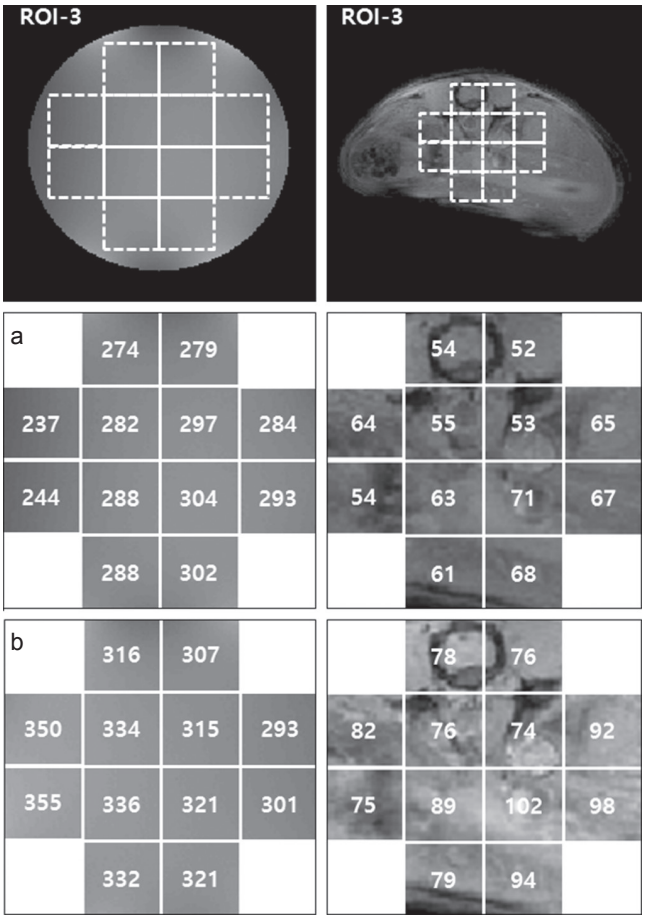

Fig 6. Mean SNR values (mean value of each white box at center slice (ROI-3)) of (**a**) SBC coil and (**b**) ABC coil obtained and compared for the cylindrical phantom (left) and *in vivo* mouse body (right).

Figure 6 shows the mean SNR values for the SBC (Fig. 6a) and ABC (Fig. 6b) coils obtained for the cylindrical phantom and *in vivo* mouse body in the central axial slice of ROI-3. The mean SNR values of the ABC and SBC coil show the inhomogeneous distribution; that is, the mean SNR slightly decreased from the central region to the peripheral region of the FLASH MR image. The averaged SNR value of the phantom in the dedicated central square area (i.e., white box) is 326.5 for the ABC coil and 292.7 for the SBC coil. In the *in vivo* mouse body comparison, the averaged SNR value of the ABC coil is 85.2 and that of the SBC coil is 60.5. Therefore, the SNR of the ABC coil is 9% and 40% higher than that of the SBC coil for the phantom and the *in vivo* mouse body, respectively.

Table 2 lists the mean values for entire SNR and FA maps for the SBC and ABC coils. In the phantom study, the FA values are similar to the two coils in the central axial slice of ROI-3 and mean SNR value of ABC coil is slightly higher than SBC coil. However, two values for the SBC coil are higher than for the ABC coil in the other four ROIs. In particular, for the 7T mouse MR image, these two evaluation factors (SNR and FA values) for the ABC coil are superior to those of the SBC coil in the central axial slice: the SNR value of the ABC coil is 49.5% higher and the FA value is 50% higher than those of the SBC coil. Therefore, although the signal sensitivity and the FA value of the ABC coil were lower than those of the SBC coil, the ABC coil has superior coil performance in the central axial slice.

Discussion

An ABC coil configuration was designed, manufactured, and tested in the 7T small-animal body MR imaging for evaluating

Table 2. Mean values of the entire SNR and FA maps for SBC and ABC coils for (**a**) cylindrical phantom and (**b**) *in vivo* mouse body MR imaging at 7T

(a)						[Unit: a.u.]
7T phantom MR image		ROI_1	ROI_2	ROI_3	ROI_4	ROI_5
SNR map (Mean)	SBC	1.59e+07	1.69e+07	1.73e+07	1.72e+07	1.60e+07
	ABC	1.29e+07	1.26e+07	1.98e+07	1.44e+07	1.40e+07
						[Unit: °]
FA map (Mean)	SBC	60.435	61.330	61.341	60.921	59.791
	ABC	56.246	56.895	61.427	58.695	56.953
(b)						[Unit: a.u.]
7T mouse MR image		ROI_1	ROI_2	ROI_3	ROI_4	ROI_5
SNR map (Mean)	SBC	9.12e+06	6.02e+06	1.05e+07	1.12e+07	9.64e+06
	ABC	7.51e+06	7.23e+06	1.57e+07	1.43e+07	1.31e+07
						[Unit: °]
FA map (Mean)	SBC	38.942	44.340	39.690	43.195	47.368
	ABC	45.055	61.200	59.990	56.280	60.393

upper raw mean values of SNR map, lower raw mean values of FA map. unit: a.u., unit: arbitrary; unit: °, unit: degree

the coil performance in terms of $|B_1|$ and $|B_1^+|$ field distribution as well as mean SNR. Higher $|B_1|$ and $|B_1^+|$ field has been achieved using the ABC coil configuration in the computational calculation and 7T experimental studies. The modification of the coil dimension by adjusting the coil geometry shows wide flexibility by controlling the field distribution. By the results of experimental studies, the artificial geometry of ABC coil showed a different field distribution as compared to the SBC coil. This phenomenon occurs from signal variance around the ER of the SBC coil whereas convex shaped $|B_1|$ distribution can be shown along the z-direction at SBC coil. We demonstrated that the ABC geometry with three separated parts increases the $|B_1|$ sensitivity in the central axial slice. The coil center exhibited superior $|B_1|$ sensitivity, but the offset BC coil region exhibited the lowest sensitivity. In the future, this ABC geometry needs to be improved for further increasing the signal sensitivity in the central axial slice as well as in the relatively separated target imaging area along the diagonal direction. If the target imaging region is positioned at a faraway location in the diagonal direction (e.g., brain and cardiac), the proposed ABC coil can be applicable.

Conclusion

In conclusion, we developed an ABC coil as a small-animal MRI body coil for 7T MRI apparatus. We performed a computational calculation and obtained MR images for the ABC coil and compared them with those of the SBC coil. The results showed that the ABC coil provided higher $|B_1|$ sensitivity due to the modified BC coil geometry. Thus, small-animal MR imaging is feasible by using this coil modification.

Acknowledgments

This study was supported by a Samsung Biomedical Research Institute grant (SMX1132851) and a National Research Foundation of Korea (NRF) grant (2016R1A2A1A05004952) funded by the Korea government (MSIP).

Conflicts of Interest

The authors have no disclosure statement.

References

1. Vaughan JT, Garwood M, Collins CM, et al. 7T vs. 4T: RF power, homogeneity, and signal-to-noise comparison in head images. Magn Reson Med 2001; 46:24–30.
2. Hoult DI, Richards RE. The signal to noise ratio of the nuclear magnetic resonance experiment. J Magn Reson 1976; 24:71–85.
3. Wald LL, Wiggins GC, Potthast A, Wiggins CJ, Triantafyllou C. Design consideration and coil comparison for 7T brain imaging. Appl Magn Reson 2005; 29:19–37.
4. Collins CM, Smith MB. Calculations of B1 distribution, SNR, and SAR for a surface coil adjacent to an anatomically-accurate human body model. Magn Reson Med 2001; 45: 692–699.
5. Ibrahim TS, Lee R, Abduljalil AM, Baertlein BA, Robitaille PM. Dielectric resonances and B(1) field inhomogeneity in UHFMRI: computational analysis and experimental findings. Magn Reson Imaging 2001; 19:219–226.
6. Collins CM, Liu W, Schreiber W, Yang QX, Smith MB. Central brightening due to constructive interference with, without, and despite dielectric resonance. J Magn Reson Imaging 2005; 21:192–196.
7. Yang QX, Wang J, Zhang X, et al. Analysis of wave behavior in lossy dielectric samples at high field. Magn Reson Med 2002; 47:982–989.
8. Alecci M, Collins CM, Wilson J, Liu W, Smith MB, Jezzard P. Theoretical and experimental evaluation of detached endcaps for 3 T birdcage coils. Magn Reson Med 2003; 49:363–370.
9. Keil B, Triantafyllou C, Hamm M, Wald LL. Design optimization of a 32-channel head coil at 7T. Proc Intl Soc Mag Reson Med 2010; 18:1493.
10. Hayse CE, Edelstein WA, Schenck JF, Mueller OM, Eash M. An efficient highly homogeneous radiofrequency coil for whole-body NMR imaging at 1.5T. J Magn Reson 1985; 63:622–628.
11. Qian Y, Zhao T, Wiggins GC, et al. Sodium imaging of human brain at 7T with 15-channel array coil. Magn Reson Med 2012; 68:1807–1814.
12. Bottomley PA, Andrew ER. RF magnetic field penetration, phase shift and power dissipation in biological tissue: implications for NMR imaging. Phys Med Biol 1978; 23:630–643.
13. Glover GH, Hayes CE, Pelc NJ, et al. Comparison of linear and circular polarization for magnetic resonance imaging. J Magn Reson 1969; 64:255–270.